Experimental and theoretical analyses of Iroko wood laminates

P. Corigliano [a], V. Crupi [a], G. Epasto [a, *], E. Guglielmino [a], N. Maugeri [a], A. Marinò [b]

[a] Department of Engineering, University of Messina, Contrada di Dio, 98166 Sant'Agata, Messina, Italy
[b] Department of Engineering and Architecture, University of Trieste, Piazzale Europa 1, 34127 Trieste, Italy

ARTICLE INFO

Article history:
Received 24 August 2016
Received in revised form
26 October 2016
Accepted 27 December 2016
Available online 28 December 2016

Keywords:
Wood-based composites
Laminated wood
Computed tomography
Ultrasonics
Wooden ship structures

ABSTRACT

This paper reports the experimental tests, which have been carried out to assess the mechanical properties of Iroko wood laminates used for the construction of a large wooden sailing ship. Three-point bending tests have been carried out on different types of specimens: laminates with 3 layers @ 0° and without scarf joints, laminates with 3 layers @ 0° having the outer layers with scarf joints, and laminates with 4 layers @ 0°/±45°/0° and no scarf joints. The tests have been performed in compliance with the current EN Standards. The analyses of the experimental data allowed the assessment of the mechanical properties of the laminated Iroko wood as well as the influence of scarf joints. The experimental results demonstrated that the presence of scarf joints only affect the strength of the glued laminate, while the stiffness properties in terms of Young modulus in bending and shear modulus, obtained applying the "method of variable support span", remain essentially the same. The investigated laminates have been also analysed using a 3D computed tomography and an ultrasonic phased array equipment in order to assess the dimensions of possible defects or voids in the adhesive and the dynamic modulus of elasticity. The tomographic measurements of the glue thickness explained the reason of the reduced strength of the scarf joints, due to the inhomogeneity of the glue bond-line. The value of the dynamic modulus of elasticity, obtained by the ultrasonic technique, is slightly higher than the value of the modulus of elasticity obtained by the bending tests. Finally, the experimental findings have been compared with those drawn from both Classical Lamination Theory and Dietz approach, obtaining a good agreement and confirming that the Dietz approach is a fast and easy way to assess the elastic properties of a laminated structure.

1. Introduction

Composite structures have peculiar properties, so that they have been widely used in the transport industry. Both laminated and sandwich polymeric composites, in particular, have been applied for many years in the shipbuilding industry, producing a large amount of waste. With the increasing focus of the recently introduced legislation on the environmental consequences, the waste issue becomes an important aspect for the shipbuilding industry. Nowadays, indeed, there is a growing interest for green materials and natural composites, like wood, and for the development of the science of biomimetics [1], which seeks to gain inspiration from the Nature to design new engineering solutions. The wood is the oldest material used for boat construction. It was traditionally used for crafts (like fishing boats, minehunters, lobster boats, sailing yachts, junks, dhows, gondolas, etc.) and recently it is considered again as a very attractive material for other types of vessels (such as inland/coastal passenger ships or megayachts) thanks also to the development of the wood technology and the progress of woodworking machines [2–4] in the last years. The knowledge of quality and mechanical properties of wooden laminates is very important, so there are several studies in literature [5–9] about mechanical tests on laminates made of different species of wood and reinforced by means of different techniques. IROKO is not the type of wood prevalent or dominant in boatbuilding, nevertheless there are some important applications: the hull of m/y "Dream Symphony", which is the largest wooden sailing yacht in the world, is built in glued laminated Iroko timber [10]. The authors investigated the mechanical properties of IROKO timber in Ref. [11]. IROKO wood is more often used in boatbuilding not as solid timber but as laminate.

Thus, aim of this research was the experimental investigation of

* Corresponding author.
E-mail addresses: pcorigliano@unime.it (P. Corigliano), crupi.vincenzo@unime.it (V. Crupi), gabriella.epasto@unime.it (G. Epasto), eguglie@unime.it (E. Guglielmino), nmaugeri@unime.it (N. Maugeri), marino@units.it (A. Marinò).

http://dx.doi.org/10.1016/j.compositesb.2016.12.049

Iroko wood laminates, with and without scarf joints, for applications in a wooden sailing ship.

Defectology and porosity pattern of the investigated panels have been analysed using 3D computed tomography (CT) and an ultrasonic phased array (UPA) equipment. The CT technique has already been applied by the authors for analysing the impact responses of laminated and sandwich composites [12–15], but in literature there are few applications to wood, especially for marine applications. The X-ray CT method was used by Li et al. [16] to measure the moisture content and its distribution on wood and wood-based products. Paris et al. [17] used micro X-ray computed tomography (XCT) to analyse the 3D adhesive penetration behaviour of different wood–adhesive bond-lines. Dackermann et al. [18] calculated the orthotropic material properties of two hardwood species, and compared the results obtained by both mechanical static tests and ultrasonic analyses.

In the present work, static tests were carried out to obtain the mechanical properties of the investigated Iroko laminates. Moreover, the experimental results were compared with the theoretical estimations based on the Classical Lamination Theory (CLT) and on the Dietz approach [19], obtaining a very good agreement.

2. Three-point bending tests on glued laminated timber parallel to grain

The mechanical characterization of glued laminated Iroko timber parallel to grain has been performed on two types of specimens by means of three-point bending tests. The three-point bending tests were carried out for applying the "method of variable support span", which allows to obtain both Young modulus in bending and shear modulus. This method is clearly described in Ref. [11], where it was applied to Iroko timber strips. A sample of specimens is made from laminates with three layers having grains at 0°, whereas the other one has similar laminates, but with the external layers joined at midspan by a 6:1-bevel-ratio scarf joint. The latter test pieces have been made in order to estimate the influence of the scarf joints on strength and stiffness. The geometry and the nominal sizes of the glued laminates test pieces are shown in Figs. 1 and 2.

The weight and the volume of all the specimens have been accurately measured. The mean density $\rho_{g,mean}$ obtained was

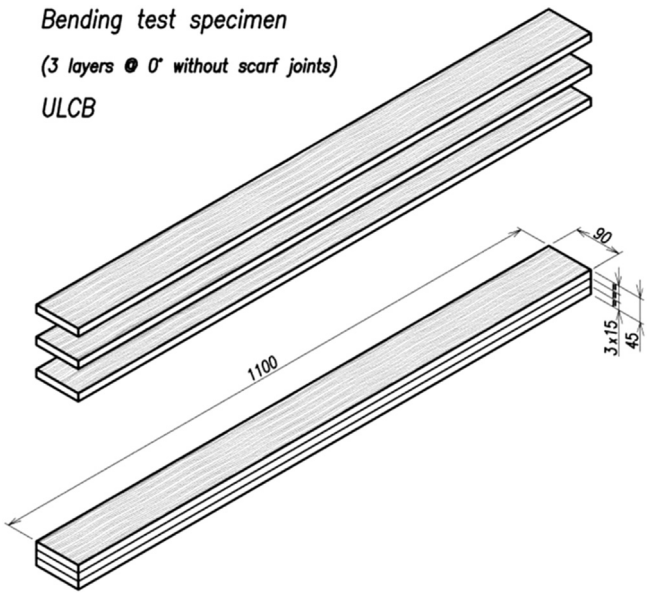

Fig. 1. Bending test specimen geometry (3 parallel-grain layers). Units: mm.

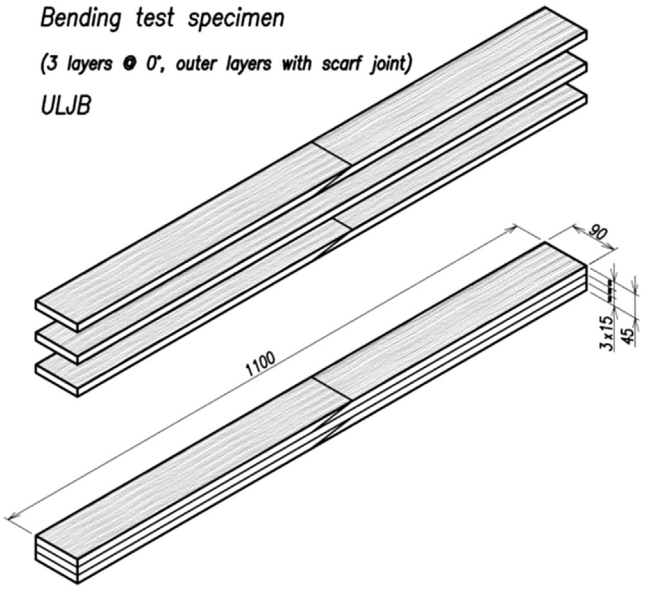

Fig. 2. Bending test specimen geometry (3 parallel-grain layers with scarf joints). Units: mm.

626 kg/m^3 for the specimens without scarf joints and 630 kg/m^3 for the ones with scarf joints at the outer layers. Also the moisture content has been measured, and came out equal to 16% for both types of test pieces.

Bending strength and stiffness have been evaluated through three-point bending tests in accordance with EN 408 Standard [20]. The bending strength $f_{m,g}$ has been determined by tests with fixed support span carried out until failure, while the bending Young modulus $E_{m,g}$ along with the shear modulus G_g have been determined through the "method of variable support span" performed within the elastic field.

The three-point bending tests have been carried out using a Controls testing machine (model 50-C1201/BFR, Fig. 3), which was found adequate for large specimens. The bending deflection at middle-span has been measured by a displacement sensor. The room temperature of the laboratory during all the tests was equal to about 20 °C and the relative humidity was about 30%.

The bending strength $f_{m,g}$ has been determined with the following formula:

$$f_{m,g} = \frac{3}{2}\frac{F_{max}\, l}{b\, h^2} \tag{1}$$

where F_{max} is the load at failure, l the support span, b the width and h the depth of the bending specimen.

In Tables 1 and 2 the results for bending strength are shown with reference to specimens without and with scarf joints, respectively. The specimens were designed using an alphanumeric label. The specimens were designed using an alphanumeric label. The letters define the laminated specimen type (with or without scarf joints) and test type (bending tests), while the numbers define the specific specimen: ULCB = Unidirectional Laminated Continuous Bending, ULJB = Unidirectional Laminated Jointed Bending.

Statistical analyses were performed to the results of the bending tests in order to define the mean and the characteristics values of some mechanical properties. The complete procedure used for the statistical analyses is clearly described in Ref. [11], where it was applied to Iroko timber specimens subjected to tensile and bending tests.

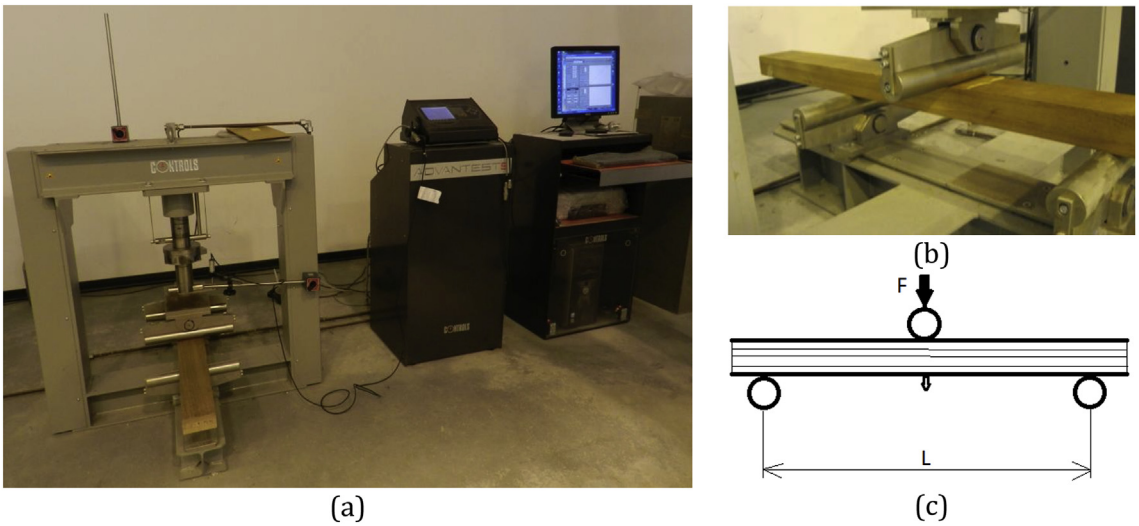

Fig. 3. Three-point bending test machine (a), (b). Scheme of bending test (c).

Table 1
Bending test results until failure (specimens without scarf joints).

Specimen	l [mm]	h [mm]	b [mm]	F_{max} [N]	$f_{m,g}$ [N/mm^2]
ULCB4	900	45.2	90.0	12696	83
ULCB6	900	45.0	90.0	11361	84
ULCB7	900	45.1	90.0	13224	98
ULCB8	900	45.2	90.3	11202	82
ULCB9	900	45.2	89.9	11637	86
ULCB10	900	45.0	90.1	14853	110
ULCB11	900	45.3	90.0	11786	86
ULCB13	900	44.9	90.0	12647	94

Table 2
Bending test results until failure (specimens with scarf joints).

Specimen	l [mm]	h [mm]	b [mm]	F_{max} [N]	$f_{m,g}$ [N/mm^2]
ULJB4	900	44.9	89.9	10517	78
ULJB5	900	45.0	90.0	9932	74
ULJB6	900	44.9	90.1	7684	57
ULJB7	900	44.9	90.0	8910	66
ULJB9	900	44.9	90.0	8585	64
ULJB10	900	45.3	90.1	7738	56
ULJB11	900	45.1	90.4	11481	84
ULJB13	900	45.1	90.0	7876	58

The statistical analyses of the experimental data reported in Tables 1 and 2 have provided the results shown in Figs. 4 and 5.

It can be observed that the presence of scarf joints does significantly decrease the bending strength. Fig. 6 shows the failure of a specimen with scarf joints (ULJB4) after the bending test.

The stiffness properties in terms of Young modulus in bending $E_{m,g}$ and shear modulus G_g have been obtained applying the "method of variable support span". In accordance with EN 408 Standard [20], for each specimen, at different support spans, is evaluated the relevant apparent modulus of elasticity $E_{m,app}$, which incorporates the mid-span shear deflection w_s within the bending deflection. In other terms, it is assumed:

$$w = w_b + w_s = \frac{1}{48}\frac{F\,l^3}{E_{m,app}\,J} \tag{2}$$

where $J = bh^3/12$ is the second moment of area about the neutral axis.

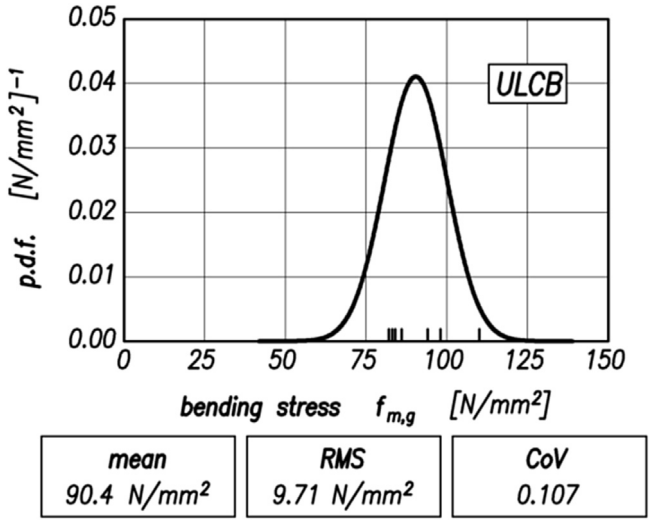

Fig. 4. Statistical analysis of bending strength results (specimens without scarf joints).

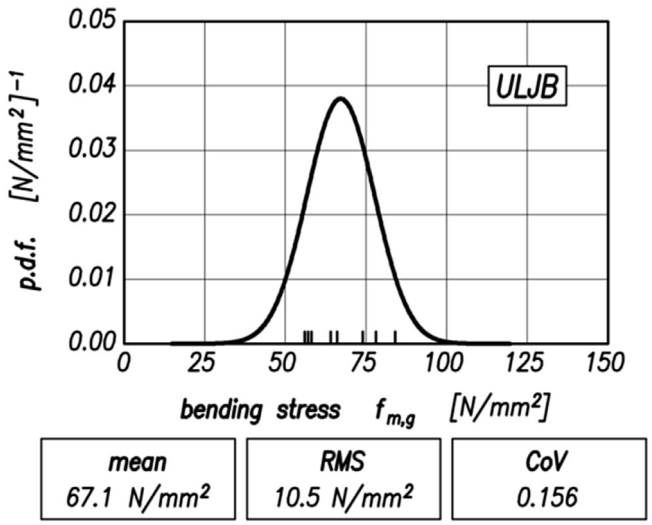

Fig. 5. Statistical analysis of bending strength results (specimens with scarf joints).

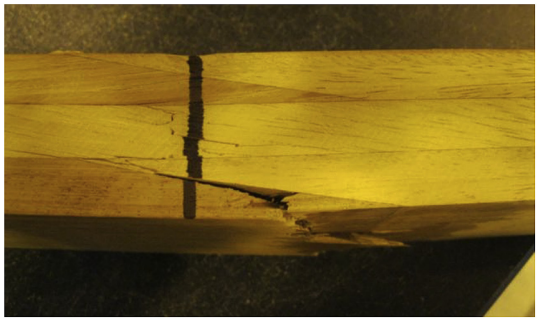

Fig. 6. Test piece with scarf joints failed after bending test.

Taking into account the expression of the true bending deflection w_b:

$$w_b = \frac{1}{48}\frac{F\,l^3}{E_{m,g}\,J} \tag{3}$$

and that for the shear deflection w_s:

$$w_s = \frac{1}{4}\frac{F\,l}{G_g\,A/\alpha} \tag{4}$$

where $A = bh$ is the cross sectional area, and α the form factor equal to 1.2 for any rectangular cross section, it is possible to derive the following relationship:

$$\frac{1}{E_{m,app}} = \frac{1}{E_{m,g}} + \frac{\alpha}{G_g}\left(\frac{h}{l}\right)^2 \tag{5}$$

which can be seen as a straight line in the variables $1/E_{m,app}$ and $(h/l)^2$. Thus, α/G_g represents the slope of the straight line, and $1/E_{m,g}$ the intercept.

With reference to the specimens without scarf joints, the results obtained for $E_{m,app}$ are reported in Table 3, whereas in Fig. 7 are plotted the straight lines drawn from the "method of variable support span". Moreover, the results of the regression analyses in terms of $E_{m,g}$ and G_g for each specimen are reported in Table 4, and the results of the statistical analysis are shown in Fig. 8.

With reference to the specimens with scarf joints at the outer layers, similar tables and figures are given: Table 5 for $E_{m,app}$, Fig. 9 for the straight lines drawn from the "method of variable support span", Table 6 for $E_{m,g}$ and G_g, and Fig. 10 for the statistical analysis of data.

The mechanical properties of the homogeneous glued laminates Iroko timber parallel to grain can be given by the 5-percentile value of the bending strength $f_{m,g,k}$, the mean bending Young modulus

Table 3
Results of bending tests by the variable span method (specimens without scarf joints).

Specimen	l[mm]	900	390	290	240
	h [mm]	$E_{m,app}$ [N/mm^2]			
ULCB4	45.2	11358	6759	4213	3200
ULCB6	45.0	10463	6632	4422	3070
ULCB7	45.1	12307	7471	5274	3762
ULCB8	45.2	11932	7019	4661	3427
ULCB9	45.2	11189	6901	4567	3275
ULCB10	45.0	14437	8603	5686	3847
ULCB11	45.3	10951	6805	4644	3101
ULCB13	44.9	11847	7481	5114	3527

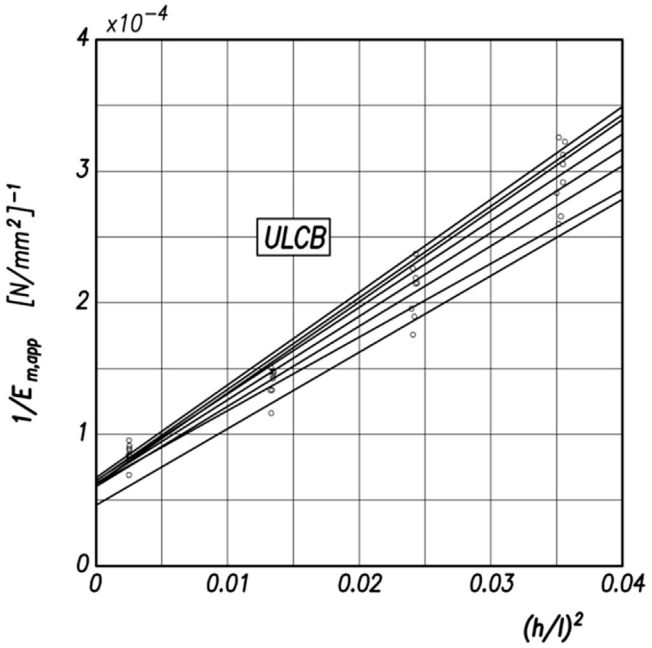

Fig. 7. Linear regression analysis of variable span method data (specimens without scarf joints).

Table 4
Results of the regression analyses method (specimens without scarf joints).

Specimen	$E_{m,g}$ [N/mm^2]	G_g [N/mm^2]
ULCB4	15422	173
ULCB6	14854	170
ULCB7	16021	215
ULCB8	15867	189
ULCB9	15381	182
ULCB10	21619	206
ULCB11	16015	173
ULCB13	16542	197

$E_{m,g,mean}$ and the mean shear modulus $G_{g,mean}$. In order to evaluate the influence of scarf joints on such properties, the experimental results obtained for specimens without and with scarf joints can be usefully compared. In Table 7 the characteristic values of strength and stiffness are put in comparison. It can be observed that the presence of scarf joints only affect the strength of the glued laminate (with a decrease of about 33%), while both bending and shear stiffness remain essentially the same.

3. Three-point bending tests on glued laminated iroko timber (4 layers @ 0°/±45°/0°)

Three-point bending tests have been performed on Iroko wood laminates for evaluating the mechanical properties. The specimens were obtained from panels consisting of 4 layers having grain orientation at 0°/±45°/0°, without scarf joints. Within each layer the timber strips are glued side by side with a circular tongue-groove joint.

The geometry and the nominal sizes of the test pieces are shown in Fig. 11.

Dimensions, weight and moisture content of all the investigated test pieces have been accurately measured. Their mean density $\rho_{g,mean}$ was about 623 kg/m^3 and the mean moisture content equal to 15%.

The bending strength in terms of applied load F_{max} at failure has

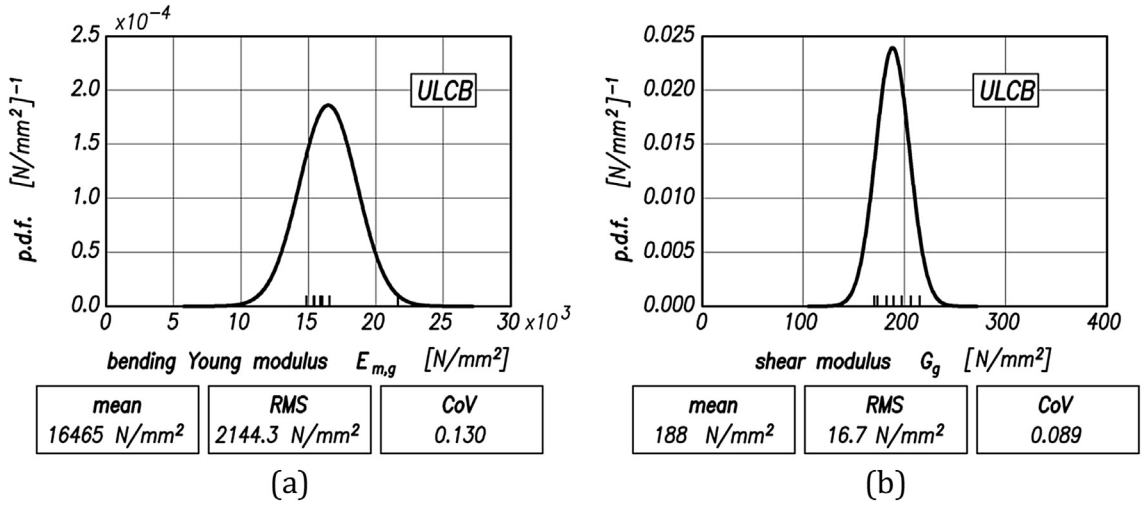

Fig. 8. Statistical analysis of three-point bending tests (specimens without scarf joints).

Table 5
Results of bending tests by the variable span method (specimens with scarf joints).

Specimen	l [mm]	900	390	290	240
	h [mm]	$E_{m,app}$ [N/mm^2]			
ULJB4	44.9	10417	6607	3834	3066
ULJB5	45.0	11963	7335	4784	3507
ULJB6	44.9	13538	8054	5068	3605
ULJB7	44.9	11733	7136	5236	3517
ULJB9	44.9	10459	6636	4433	3006
ULJB10	45.3	12121	7479	4988	3678
ULJB11	45.1	12880	8205	4993	3626
ULJB13	45.1	11953	7068	4716	3505

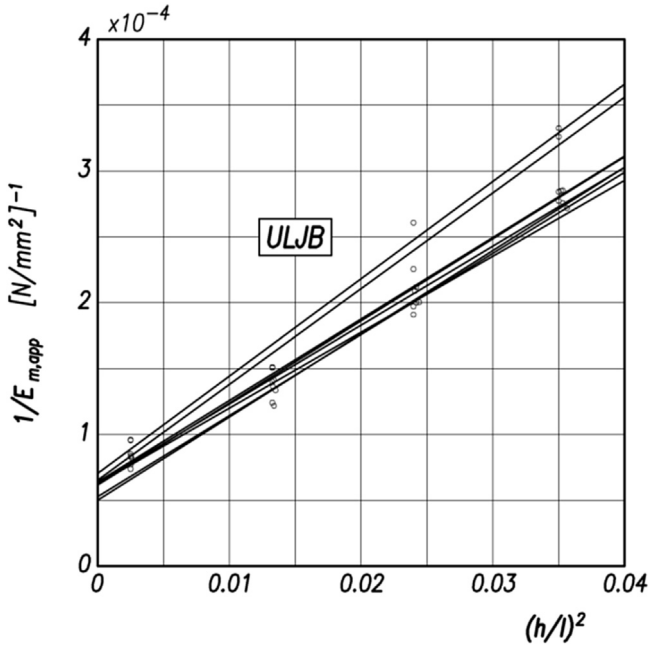

Fig. 9. Linear regression analysis of variable span method data (specimens with scarf joints).

been determined by three-point bending tests with fixed support span. Table 8 reports the values of maximum load F_{max} at failure,

Table 6
Results of the regression analyses method (specimens with scarf joints).

Specimen	$E_{m,g}$ [N/mm^2]	G_g [N/mm^2]
ULJB4	14166	162
ULJB5	16231	193
ULJB6	19937	190
ULJB7	15816	200
ULJB9	15292	165
ULJB10	15986	208
ULJB11	18955	195
ULJB13	15614	194

along with span l, total depth h and width b of each test piece investigated (MLCB = Multidirectional Laminated Continuous Bending).

The results of the statistical analysis of the bending loads at failure F_{max} reported in Table 8 are summarized in Fig. 12.

An Iroko wood laminate (4 layers @ 0°/±45°/0°) specimen failed after a three-point bending test is shown in Fig. 13.

The stiffness properties in terms of bending Young modulus $E_{m,g}$ and shear modulus G_g of the whole laminate have been determined through three-point bending tests by the "method of variable support span" performed on eight specimens within the elastic field. The calculated values of the apparent moduli of elasticity $E_{m,app}$ are reported in Table 9.

The regression straight lines from which to obtain the bending Young modulus $E_{m,g}$ (intercept is $1/E_{m,g}$) and the shear modulus G_g(slope is α/G_g) are traced in Fig. 14. The stiffness properties so obtained are reported in Table 10, while the results of the statistical analyses are shown in Fig. 15.

4. Theoretical approaches for flexural stiffness and strength of a laminate

The flexural stiffness of a laminate can be determined by a theoretical approach based on the Classical Lamination Theory or on the A.G.H. Dietz method [19]. Both approaches have been applied to the previously investigated Iroko wood laminates (4 layers @ 0°/±45°/0°) denoted by MLCB, and the bending strength has been determined. The theoretical results so obtained have been then compared with the experimental data.

In order to complete the mechanical characterization of the Iroko hardwood, it can be used equations as specified in EN 338

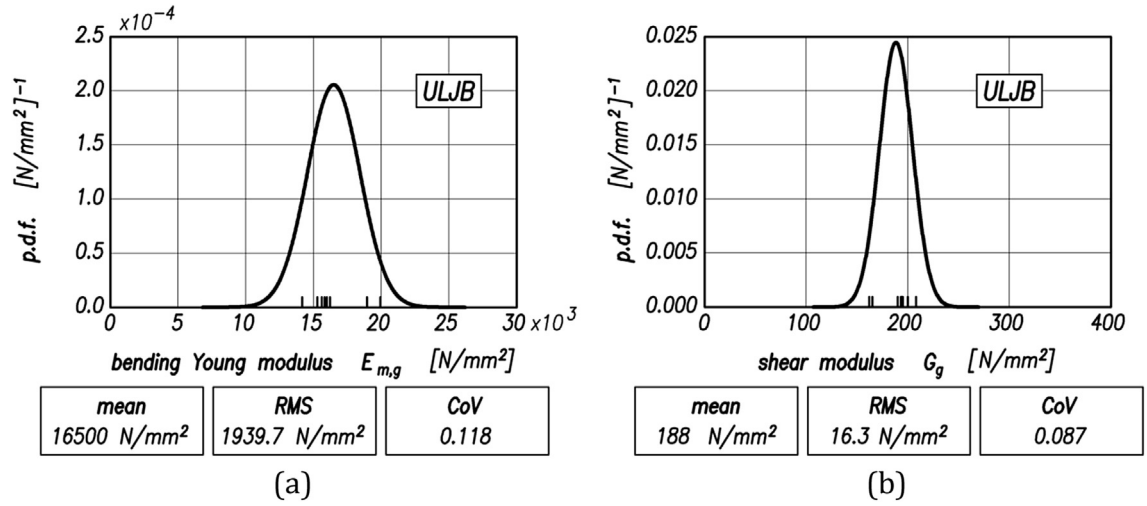

Fig. 10. Statistical analysis of three-point bending tests (specimens with scarf joints).

Table 7
Comparison between glued laminates without and with scarf joints.

Specimen	$f_{m,g,k}$ [N/mm^2]	$E_{m,g,mean}$ [N/mm^2]	$G_{g,mean}$ [N/mm^2]
ULCB (without scarf joints)	74.4	16465	188
ULJB (with scarf joints)	49.8	16500	188

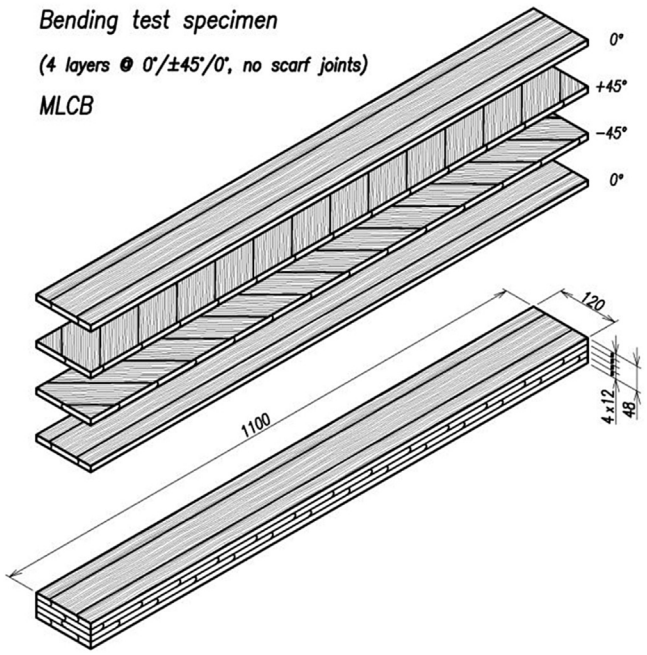

Fig. 11. Bending test specimen geometry (4 layers @ 0°/±45°/0°). Units: mm.

Standard [21], according to which the in-plane mean modulus of elasticity perpendicular to grain E_2 and the mean shear modulus G_{12} can be expressed proportionally to the in-plane mean modulus of elasticity parallel to grain E_1 as follows:

$$E_2 = E_1/15 \tag{6}$$

$$G_{12} = E_1/16 \tag{7}$$

Table 8
Bending test results until failure (4 layers @ 0°/±45°/0°).

Specimen	l [mm]	h [mm]	b [mm]	F_{max} [N]
MLCB7	900	47.7	120.9	14832
MLCB8	900	47.7	120.7	12660
MLCB9	900	48.0	120.4	12408
MLCB10	900	47.7	120.5	14638
MLCB11	900	48.1	120.5	15020
MLCB12	900	48.0	120.7	14426
MLCB13	900	47.8	120.5	13532
MLCB14	900	47.9	120.7	16643
MLCB15	900	48.0	120.5	14168
MLCB16	900	48.0	120.4	14604
MLCB17	900	48.0	120.7	16036
MLCB18	900	48.0	120.5	15408
MLCB19	900	47.9	120.8	14392
MLCB20	900	48.1	120.5	15000
MLCB21	900	47.8	120.5	14776
MLCB22	900	47.7	120.7	15755
MLCB23	900	47.8	120.8	15350
MLCB24	900	47.7	120.7	13449
MLCB26	900	48.1	120.5	16302
MLCB27	900	47.9	120.8	16305
MLCB28	900	48.0	120.5	17224
MLCB29	900	47.9	120.6	16048
MLCB30	900	47.9	120.3	15576

For Iroko wood the major Poisson ratio ν_{12} can be assumed equal to 0.50, and the minor Poisson ratio ν_{21} can be calculated by the following equation valid for orthotropic materials:

$$\nu_{21} = \nu_{12} E_2/E_1 \tag{8}$$

The in-plane modulus of elasticity E_1 can be assumed equal to the mean bending modulus $E_{m,g,mean}$ previously obtained by the three-point bending tests carried out on homogenous Iroko laminates made of 3 glued layers with grain at 0° and without scarf joints (see ULCB specimens in Table 7), thus:

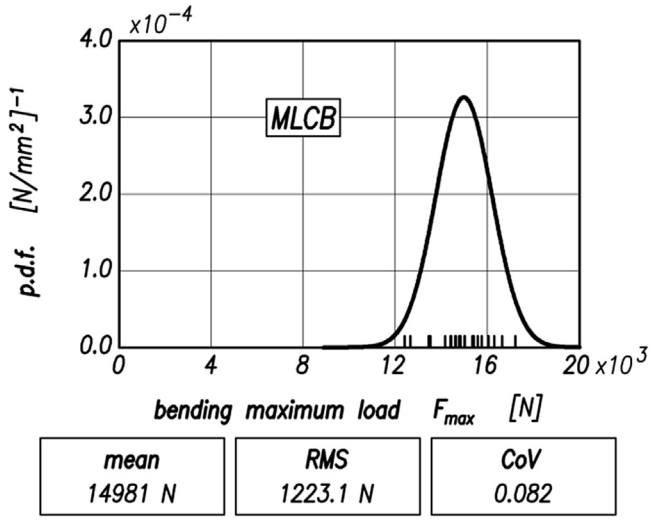

Fig. 12. Statistical analysis of bending strength results (4 layers @ 0°/±45°/0°).

the Tsai-Pagano invariants:

$$\begin{aligned} U_1 &= 0.125\,(3Q_{11} + 3Q_{22} + 2Q_{12} + 4Q_{66}) \\ U_2 &= 0.5\,(Q_{11} - Q_{22}) \\ U_3 &= 0.125\,(Q_{11} + Q_{22} - 2Q_{12} - 4Q_{66}) \\ U_4 &= 0.125\,(Q_{11} + Q_{22} + 6Q_{12} - 4Q_{66}) \\ U_5 &= 0.125\,(Q_{11} + Q_{22} - 2Q_{12} + 4Q_{66}) \end{aligned} \tag{10}$$

whose numerical values [N/mm^2] are reported in Table 12.

and then to calculate the transformed stiffness matrices $[\overline{Q}]_\vartheta$ as follows:

$$\left[\overline{Q}\right]_\vartheta = \begin{bmatrix} \overline{Q}_{11} & \overline{Q}_{12} & \overline{Q}_{16} \\ & \overline{Q}_{22} & \overline{Q}_{26} \\ \text{sim.} & & \overline{Q}_{66} \end{bmatrix}_\vartheta \tag{11}$$

where

Fig. 13. Test piece failed after a bending test (4 layers @ 0°/±45°/0°).

Table 9
Results of bending tests by the variable span method (4 layers @ 0°/±45°/0°).

Specimen	l [mm]	940	420	310	260
	h [mm]	$E_{m,app}$ [N/mm^2]			
MLCB9	48.0	9222	6013	4089	3066
MLCB10	47.7	9913	6438	4093	3150
MLCB11	48.1	10160	6420	4009	2901
MLCB12	48.0	9850	6425	4313	3090
MLCB13	47.8	10003	6460	4135	2986
MLCB14	47.9	11596	7067	4266	2997
MLCB15	48.0	9920	6494	4171	2979
MLCB16	48.0	9751	6501	4393	3126

$$E_1 = 16465\text{N}/\text{mm}^2$$

With reference to the laminae of MLCB laminates (Fig. 11) it is possible to calculate the stiffness matrix $[Q]_{(1,2)}$ for a plane stress state in the *1,2* principal material axes:

$$[Q]_{(1,2)} = \begin{bmatrix} Q_{11} & Q_{12} & 0 \\ & Q_{22} & 0 \\ \text{sim.} & & Q_{66} \end{bmatrix} = \begin{bmatrix} E_1/\Delta & \nu_{21}E_1/\Delta & 0 \\ & E_2/\Delta & 0 \\ \text{sim.} & & G_{12} \end{bmatrix} \tag{9}$$

where: $\Delta = 1 - \nu_{12}\nu_{21}$

The numerical values [N/mm^2] obtained for the material stiffnesses are reported in Table 11.

Successively, to take into account the different orientation ϑ of each lamina with respect to the *x*-axis along the length of the beam ($\vartheta = 0°/\pm45°/0°$), the relevant transformed stiffness matrix $[\overline{Q}]_\vartheta$ is determined. For this purpose, it is convenient at first to introduce

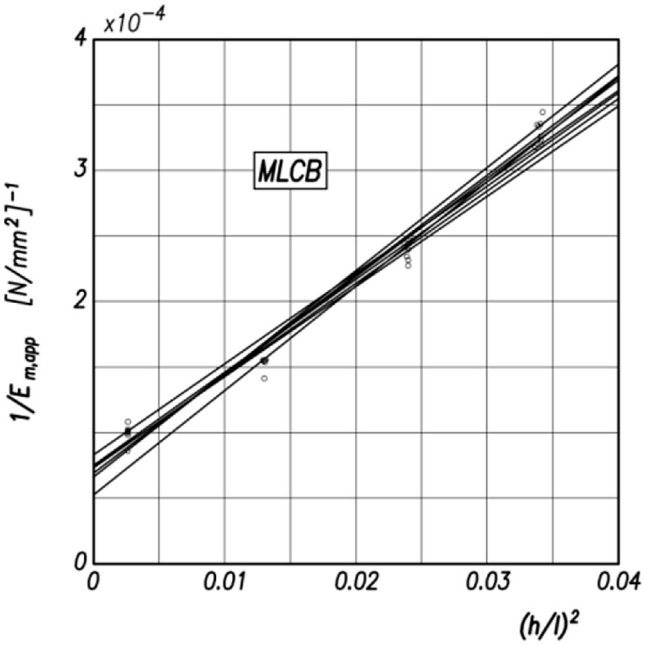

Fig. 14. Linear regression analysis of variable span method data (4 layers @ 0°/±45°/0°).

Table 10
Results of the regression analyses method (4 layers @ 0°/±45°/0°).

Specimen	$E_{m,g}$ [N/mm^2]	G_g [N/mm^2]
MLCB9	11984	173
MLCB10	13296	169
MLCB11	15042	153
MLCB12	13631	170
MLCB13	14407	158
MLCB14	18901	151
MLCB15	14417	160
MLCB16	13494	174

Table 13
Transformed stiffnesses of the laminae.

	$\vartheta = 0°$	$\vartheta = 45°$	$\vartheta = -45°$
$\overline{Q}_{11}$	16744	5773.2	5773.2
$\overline{Q}_{22}$	1116.3	5773.2	5773.2
$\overline{Q}_{12}$	558.14	3715.1	3715.1
$\overline{Q}_{66}$	1029.1	4186	4186
$\overline{Q}_{16}$	0	3906.9	−3906.9
$\overline{Q}_{26}$	0	3906.9	−3906.9

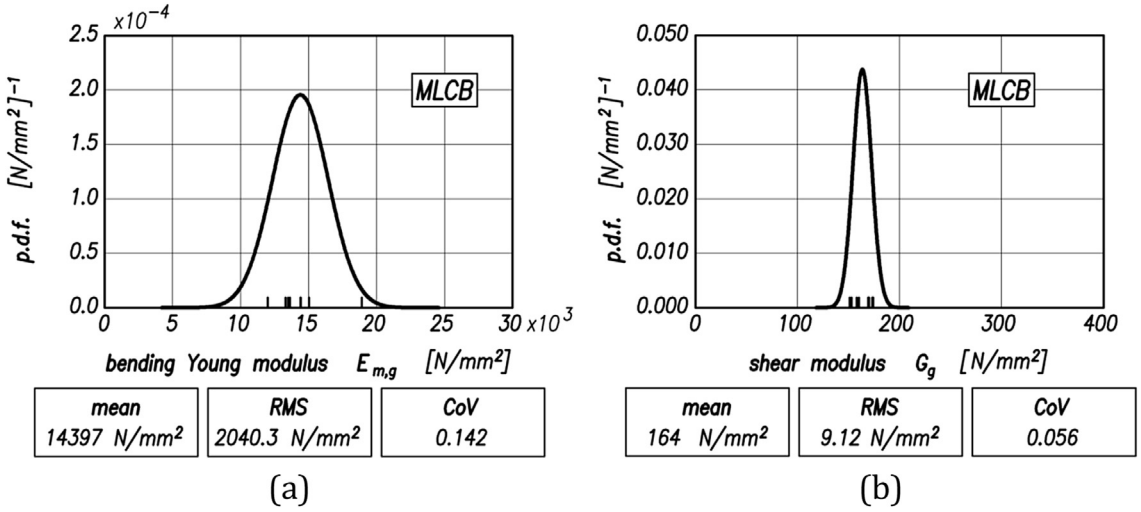

Fig. 15. Statistical analysis of three-point bending tests (4 layers @ 0°/±45°/0°).

Table 11
Stiffnesses in the principal material axis of the laminae.

Q_{11}	Q_{22}	$Q_{12} = Q_{21}$	Q_{66}
16744	1116.3	558.14	1029.1

Table 12
Tsai-Pagano invariants of the laminae.

U_1	U_2	U_3	U_4	U_5
7351.7	7813.9	1578.5	2136.6	2607.5

$$\begin{aligned}
\overline{Q}_{11} &= U_1 + U_2\cos(2\vartheta) + U_3\cos(4\vartheta)\\
\overline{Q}_{22} &= U_1 - U_2\cos(2\vartheta) + U_3\cos(4\vartheta)\\
\overline{Q}_{12} &= U_4 - U_3\cos(4\vartheta)\\
\overline{Q}_{22} &= U_1 - U_2\cos(2\vartheta) + U_3\cos(4\vartheta)\\
\overline{Q}_{66} &= U_5 - U_3\cos(4\vartheta)\\
\overline{Q}_{16} &= 0.5\,U_2\sin(2\vartheta) + U_3\sin(4\vartheta)\\
\overline{Q}_{26} &= 0.5\,U_2\sin(2\vartheta) - U_3\sin(4\vartheta)
\end{aligned} \tag{12}$$

The numerical results in [N/mm^2] for the transformed stiffnesses of the material of the laminae forming the analysed MLCB laminate are reported in Table 13.

It is possible now to evaluate the flexural stiffness of the laminate. The investigated Iroko wood laminate MLCB has an overall depth $h = 48$ mm, and each lamina has a thickness $t = 12$ mm.

In the Classical Lamination Theory the constitutive equation of a laminate, with reference to a unit width, is given by the following matrix expression:

$$\begin{Bmatrix} \boldsymbol{N} \\ \boldsymbol{M} \end{Bmatrix} = \begin{bmatrix} \boldsymbol{A} & \boldsymbol{B} \\ \boldsymbol{B} & \boldsymbol{D} \end{bmatrix} \begin{Bmatrix} \boldsymbol{\varepsilon}^o \\ \boldsymbol{\chi} \end{Bmatrix} \tag{13}$$

or in extended form:

$$\begin{Bmatrix} N_x \\ N_y \\ N_{xy} \\ M_x \\ M_y \\ M_{xy} \end{Bmatrix} = \begin{bmatrix} A_{11} & A_{12} & A_{16} & B_{11} & B_{12} & B_{16} \\ A_{12} & A_{22} & A_{26} & B_{12} & B_{22} & B_{26} \\ A_{16} & A_{26} & A_{66} & B_{16} & B_{26} & B_{66} \\ B_{11} & B_{12} & B_{16} & D_{11} & D_{12} & D_{16} \\ B_{12} & B_{22} & B_{26} & D_{12} & D_{22} & D_{26} \\ B_{16} & B_{26} & B_{66} & D_{16} & D_{26} & D_{66} \end{bmatrix} \begin{Bmatrix} \varepsilon_x^o \\ \varepsilon_y^o \\ \gamma_{xy}^o \\ \chi_x \\ \chi_y \\ \chi_{xy} \end{Bmatrix} \tag{14}$$

The sub-vectors $\boldsymbol{N}$ and $\boldsymbol{M}$ are the tensile/shear forces and the bending/twisting moments per unit length, whereas $\boldsymbol{\varepsilon}^o$ and $\boldsymbol{\chi}$ are the in-plane linear/angular strains and the bending/twisting curvatures of the middle surface of the laminate, respectively.

$\boldsymbol{A}$ is the in-plane extentional stiffness matrix, $\boldsymbol{B}$ is the bending-extension coupling stiffness matrix, and $\boldsymbol{D}$ is the bending stiffness matrix. The coefficients A_{ij}, B_{ij} and D_{ij} are function of the thickness, orientation, stacking sequence and material properties of the laminae; their expressions are:

$$A_{ij} = \sum_{k=1}^{n} \left(\overline{Q}_{ij}\right)_k (z_k - z_{k-1}) \tag{15}$$

$$B_{ij} = \frac{1}{2}\sum_{k=1}^{n}\left(\overline{Q}_{ij}\right)_k\left(z_k^2 - z_{k-1}^2\right) \tag{16}$$

$$D_{ij} = \frac{1}{3}\sum_{k=1}^{n}\left(\overline{Q}_{ij}\right)_k\left(z_k^3 - z_{k-1}^3\right) \tag{17}$$

where n is the number of laminae, z_k and z_{k-1} are the face coordinates of the k-th lamina from mid-plane of the laminate.

For the case-study (Iroko wood laminate MLCB) the stiffness matrix is:

$$\begin{bmatrix} A & B \\ B & D \end{bmatrix} = \begin{bmatrix} 5.4041\cdot10^{5} & 1.0256\cdot10^{5} & 0 & -4.6566\cdot10^{-10} & -1.4552\cdot10^{-11} & -5.6260\cdot10^{5} \\ 1.0256\cdot10^{5} & 1.6535\cdot10^{5} & 0 & -1.4552\cdot10^{-11} & 0 & -5.6260\cdot10^{5} \\ 0 & 0 & 1.2516\cdot10^{5} & -5.6260\cdot10^{5} & -5.6260\cdot10^{5} & 0 \\ -4.6566\cdot10^{10} & -1.4552\cdot10^{-11} & -5.6260\cdot10^{5} & 1.4167\cdot10^{8} & 8.7806\cdot10^{6} & 0 \\ -1.4552\cdot10^{-11} & 0 & -5.6260\cdot10^{5} & 8.7806\cdot10^{6} & 1.5652\cdot10^{7} & 0 \\ -5.6260\cdot10^{5} & -5.6260\cdot10^{5} & 0 & 0 & 0 & 1.3121\cdot10^{7} \end{bmatrix}$$

The compliance equations of the laminate are obtained inverting the stiffness equation (13):

$$\begin{Bmatrix} \boldsymbol{\varepsilon}^o \\ \boldsymbol{\chi} \end{Bmatrix} = \begin{bmatrix} \boldsymbol{A} & \boldsymbol{B} \\ \boldsymbol{B} & \boldsymbol{D} \end{bmatrix}^{-1} \begin{Bmatrix} \boldsymbol{N} \\ \boldsymbol{M} \end{Bmatrix} = \begin{bmatrix} \boldsymbol{\alpha} & \boldsymbol{\beta} \\ \boldsymbol{\beta}^T & \boldsymbol{\delta} \end{bmatrix} \begin{Bmatrix} \boldsymbol{N} \\ \boldsymbol{M} \end{Bmatrix} \tag{18}$$

The numerical results for the investigated Iroko laminate is:

$$\begin{bmatrix} \alpha & \beta \\ \beta^T & \delta \end{bmatrix} = \begin{bmatrix} 2.1154\cdot10^{-6} & -1.1748\cdot10^{-6} & 2.7021\cdot10^{-23} & 7.0008\cdot10^{-24} & -9.8940\cdot10^{-25} & 4.0329\cdot10^{-8} \\ -1.1748\cdot10^{-6} & 7.7334\cdot10^{-6} & -1.3226\cdot10^{-23} & -3.1314\cdot10^{-24} & 1.8901\cdot10^{-25} & 2.8123\cdot10^{-7} \\ 2.7021\cdot10^{-23} & -1.3226\cdot10^{-23} & 9.5699\cdot10^{-6} & 1.7285\cdot10^{-8} & 3.3428\cdot10^{-7} & 5.9152\cdot10^{-25} \\ 7.0008\cdot10^{-24} & -3.1314\cdot10^{-24} & 1.7285\cdot10^{-8} & 7.3439\cdot10^{-9} & -3.4984\cdot10^{-9} & 1.6592\cdot10^{-25} \\ -9.8940\cdot10^{-25} & 1.8901\cdot10^{-25} & 3.3428\cdot10^{-7} & -3.4984\cdot10^{-9} & 7.7866\cdot10^{-8} & -3.432\cdot10^{-26} \\ 4.0329\cdot10^{-8} & 2.8123\cdot10^{-7} & 5.9152\cdot10^{-25} & 1.6592\cdot10^{-25} & -3.4320\cdot10^{-26} & 9.0004\cdot10^{-8} \end{bmatrix}$$

In the stress resultants vector $\{N_x\ N_y\ N_{xy}\ M_x\ M_y\ M_{xy}\}^T$ of the case study only $M_x \neq 0$, thus the bending curvature χ_x of the beam is given by:

$$\chi_x = M_x/D_x = \delta_{11}M_x \tag{19}$$

Therefore, within the Classical Lamination Theory (CLT), the flexural stiffness in x-direction of the unit-width laminate is:

$$D_{x_{CLT}} = 1/\delta_{11} = 1.3617\cdot108\text{N mm}^2\big/\text{mm} \tag{20}$$

An approximate value for the flexural stiffness D_x can be obtained by the approach suggested by professor A.G.H. Dietz. In such an approach the geometrical area of each lamina is weighted with its own in-plane Young modulus of elasticity E_x along the length of the beam (i.e., x-axis). Successively, the neutral axis of the laminate is properly positioned taking into account the elastic weights $(E_x)_k$ of each lamina. The flexural stiffness D_x is given by the weighted second moment of area of the laminate cross-section about the neutral axis. For an anti-symmetric laminate, like the one considered, the neutral plane coincides with the mid-plane, and so with reference to an unit-width beam D_x becomes:

$$D_{x_{DIETZ}} = \frac{1}{3}\sum_{k=1}^{n}(E_x)_k\left(z_k^3 - z_{k-1}^3\right) \tag{21}$$

For orthotropic laminae with an off-axis orientation ϑ, the relationship between E_x and the elastic properties referred to the principal axes of the material is:

$$\frac{1}{E_x} = \frac{(\cos\vartheta)^4}{E_1} + \left(\frac{1}{G_{12}} - \frac{2\nu_{12}}{E_1}\right)(\sin\vartheta)^2(\cos\vartheta)^2 + \frac{(\sin\vartheta)^4}{E_2} \tag{22}$$

Thereby, with reference to the investigate case study, it is:

$$D_{x_{DIETZ}} = 1.3522\cdot108\text{N mm}^2\big/\text{mm}$$

Correspondingly, it is possible to calculate the bending modulus of elasticity in x-direction for the investigated laminate as:

$$E_{m,x} = 12D_x\big/h^3 \tag{23}$$

It is worth to compare the theoretical bending modulus of elasticity obtained by both Classical Lamination Theory and Dietz approach with that obtained through the "method of variable support span" carried out by three-point bending tests described in Section 3. Table 14 summarized the numerical results, and it is possible to detect very small differences.

Besides the elastic properties of the investigated laminate, the bending strength can also be verified. From bending tests carried

Table 14
Bending modulus of elasticity for MLCB laminate.

Theoretical value by CLT	$E_{m_{CLT}} = 14775\text{N/mm}^2$
Theoretical value by Dietz	$E_{m_{DIETZ}} = 14672\text{N/mm}^2$
Experimental value by tests	$E_{m,g_{EXP.}} = 14397\text{N/mm}^2$

Table 15
Bending stress at failure of investigated ULCB laminates.

Mean bending stress	$f_{m,g,mean} = 90.4\text{N/mm}^2$
Characteristic bending stress	$f_{m,g,k} = 74.4\text{N/mm}^2$

Table 16
Calculated maximum bending stress at failure for MLCB laminates.

Value by CLT	$f_{m,max_{CLT}} = 81.5\text{N/mm}^2$
Value by Dietz	$f_{m,max_{DIETZ}} = 82.1\text{N/mm}^2$
Value by experimental tests	$f_{m,max_{EXP.}} = 83.7\text{N/mm}^2$

out until failure on the laminates denoted ULCB (see Fig. 4 and Table 7) have been found both a mean and a characteristic (5-percentile) bending stress for the investigated Iroko wood as summarized in Table 15.

Those values can be taken as reference in order to verify the bending stress at failure of MLCB laminates. The three-point bending tests carried out at fixed support span ($l = 900$ mm) on MLCB specimens have given a mean maximum load at failure F_{max} equal to 14981 N, which corresponds a bending moment equal to:

$$M_{max} = F_{max}\, l/4 = 3.3707 \cdot 106\text{Nmm}$$

With reference to MLCB laminates, the bending stress at outer

Table 17
Parameters of the tomographic investigation.

Focal spot size [μm]	X-ray voltage [kV]	X-ray current [mA]	Number of projections	Integration time [ms]	Voxel size [mm^3]	Image size [pixels]	Cu filter [mm]
250	140	1.2	1440	250	50	1888 × 1888	0.5

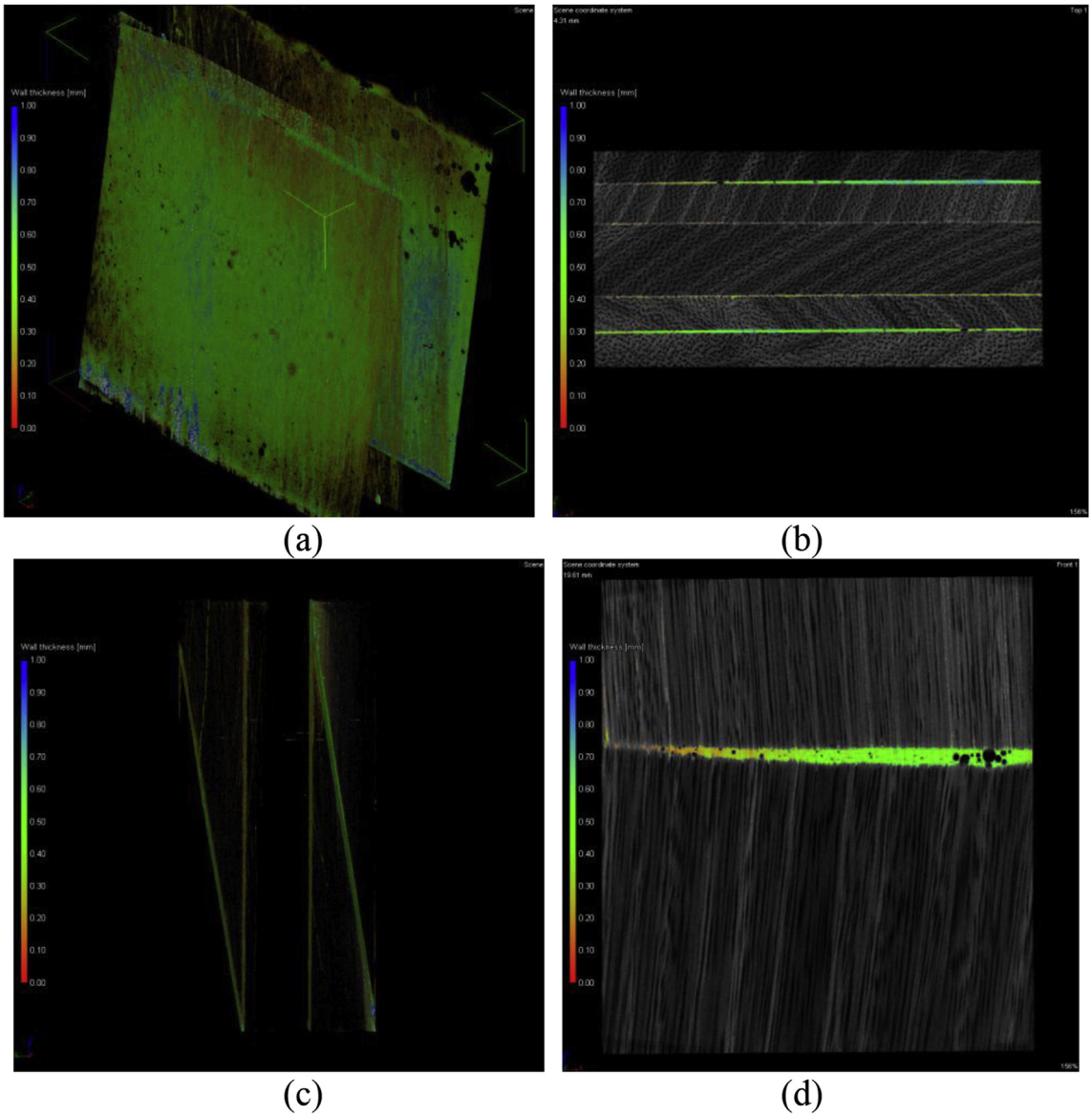

Fig. 16. Tomographic analysis of a scarf joint.

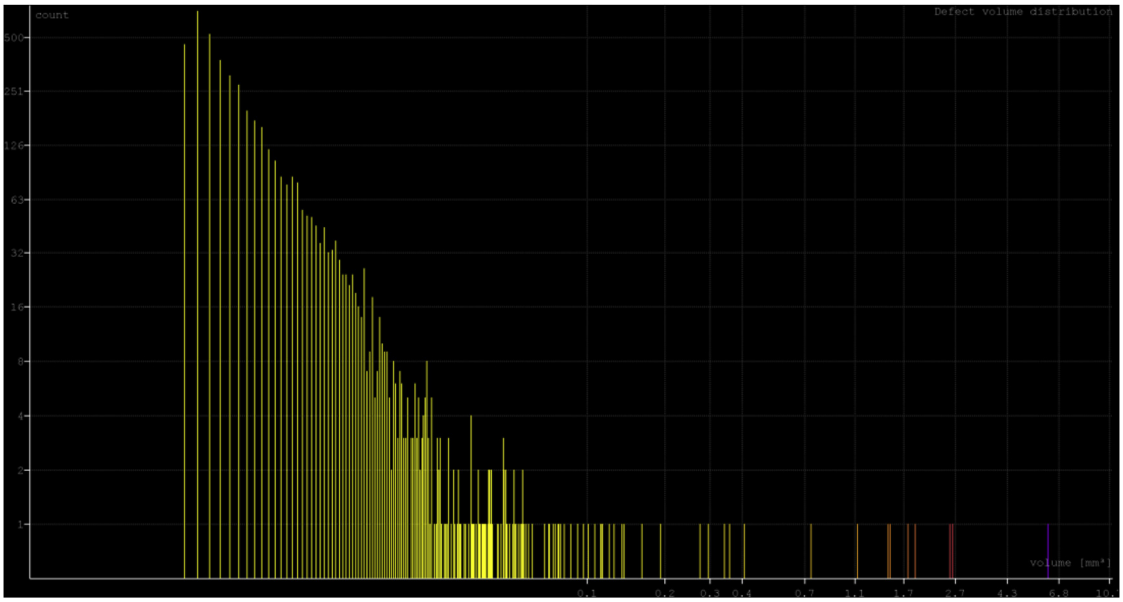

Fig. 17. Porosity detection by tomographic analysis with distribution of the pore size.

layers, which have the in-plane modulus of elasticity $E_x = E_1$, can be evaluated as follows:

$$f_{m,max} = \frac{M_{max}}{b\, D_x} E_1 \frac{h}{2} \tag{24}$$

where $b = 120° = 120$ mm is the actual width of the specimen, and D_x the flexural stiffness of the unit-width laminate. The theoretical values of the flexural stiffness have been already evaluated, whereas the value of D_x that stems from the experimental results can be determined in this manner:

$$D_{x_{EXP.}} = E_{m,g_{EXP.}}\, h^3 \big/ 12 = \; 1.3268 \cdot 10^8 \text{N mm}^2 \big/ \text{mm} \tag{25}$$

In Table 16, the maximum bending stresses evaluated by formula (24), according the various determinations for the flexural stiffness, are reported.

The values obtained for $f_{m,max}$ have to be compared with those reported in Table 15, and the theoretical estimations can be considered more than satisfactory.

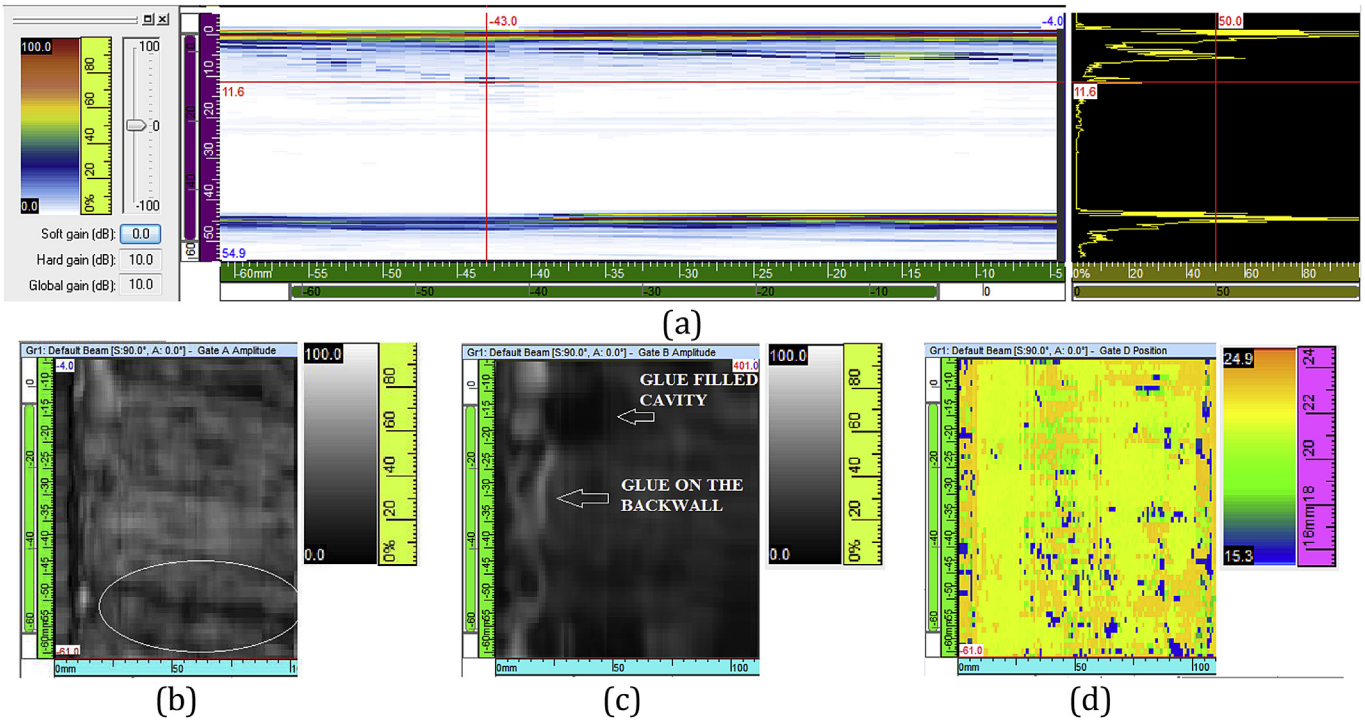

Fig. 18. B-scan (a) and C- scans (b, c, d) of a portion of the scarf joint obtained by UPA.

Table 18
MOE values and mean longitudinal wave velocities from ultrasonic test.

τ [μs]	h [mm]	V_l [m/s]	ρ [kg/m^3]	MOE [GPa]
17.4	45	5172.4	630	16.9

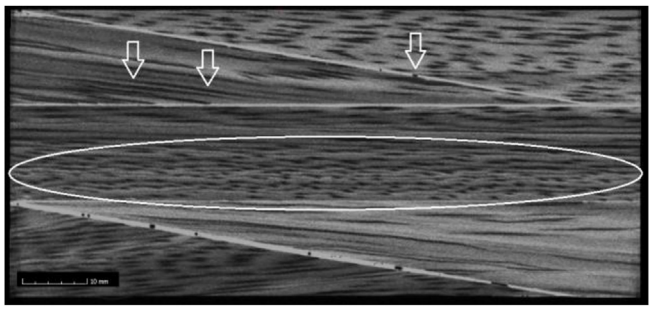

Fig. 19. Cross sectional tomogram of the scarf joint.

The good achievement between the mechanical properties predicted by the Dietz method and the experimental results (Tables 14 and 16) demonstrates that this theoretical approach is a rapid and easy way to assess the mechanical properties of laminated wood, which are very important for the design of wooden laminated structures.

5. Non-destructive tests for wooden scarf-jointed laminates

As proved by the mechanical tests, the presence of scarf joints significantly decreases the bending strength. Thus, non-destructive tests, (3D computed tomography and ultrasonic phased array) were carried out in order to evaluate and quantify possible defects and porosities in the glue, otherwise undetectable by a visual inspection, and to measure the thickness of the glue and the density variations in the wood.

Some specimens were cut in order to investigate the zone of the scarf joint using the 3D Computed Tomography (CT) system Y.CT Vario. The CT system is based on a variable focal-spot size technology and creates the cross-section images of 3D objects using cone-beam X-rays. During the scan, the sample was turned at a rate of 0.5°/s for each projection until a full rotation of 360° was achieved. In Table 17 the parameters of the CT scans used in this investigation are reported.

Fig. 16 shows the tomographic analysis of a scarf joint (specimen designated as ULJB), confirming that the CT system is an useful tool for detecting defects in wood. As shown by means of the measurements of the glue thickness, a reason of the reduced mechanical strength of the scarf joints could be found in the inhomogeneity of the glue bond-line itself. It is worth mentioning that in the analysed specimens there was a good penetration of the glue (Fig. 16c).

The defect detection and the porosity measurements underline not only the high quality of the bonding, with a porosity of 0.45%, but also the small size of the pores (Fig. 17).

The ultrasonic wave velocity and the dynamic modulus of elasticity (MOE) of the scarf joints were measured using an Ultrasonic Phased Array (UPA) equipment from Olympus (Tomoscan Focus LT) with its inspection software TomoView. A linear probe, 64 elements at 3.5 MHz (3.5L64-NW1, 64 mm aperture, 1 mm pitch, 7 mm elevation) equipped with VersaMOUSE scanner, was used. By using UPA technique and adjusting the gain of the input signal, good results can be obtained. The ultrasonic wave velocity was calculated by identifying the arrival time of the back-wall echo (Fig. 18). The measure was carried out in a section without flaws, as shown by CT analyses. The UPA can be useful for detecting defects (both in wood and in the adhesive sections) and for assessing the ultrasonic wave velocity by assuming that the glue does not affect the time-of-flight value [18].

Some preliminary ultrasonic tests allowed the calculation of the dynamic MOE by means of the relationship that shows the dependence of the MOE by the velocity of an elastic wave traveling through an orthotropic wood, the Poisson's ratio and the density of the tested wood; the pertinent equation can be found in Ref. [22]. Generally, the influence of the Poisson's ratio can be neglected, and the simplified relationship valid for isotropic materials can be considered [18]:

$$MOE = \rho\, V_l^2 \tag{26}$$

where V_l is the longitudinal ultrasonic wave velocity of the specimen (along the grains) and ρ is the density based on the mass-to-volume ratio of the specimen at 12% moisture content.

In Table 18 the measured values are reported, where h is the depth of the specimen and τ the travel time of the ultrasonic wave.

The result, obtained by the ultrasonic technique, is in agreement with the values reported in Table 7, and shows that the value of the dynamic MOE is slightly higher than the static one.

In Fig. 18a it is reported the cross sectional B-scan that provides a

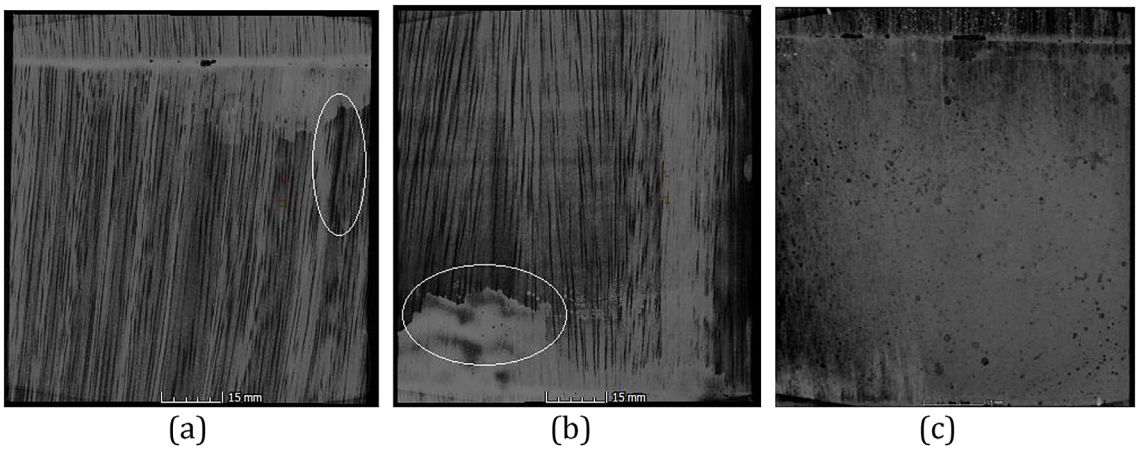

Fig. 20. Tomographic slices of the near surface (a), the bottom surface (b) and the porosity (c) shown in Fig. 18d.

detailed view of the glue line and of some defects or discontinuity at the glue-wood interface. The same study was carried out and confirmed by CT analysis. In Fig. 19, the arrows indicate a cavity at the interface, while the closed line encloses a zone of more low-density wood in the lamina at 20÷25 mm of depth.

The results of UPA C-scans were compared with CT images, confirming the results of the tomographic analyses (Fig. 20 a, b and c, respectively).

For the specimens without scarf joint (designated as ULCB), the tomographic analyses didn't show any significant defect in the glue region (Fig. 21b). Also for this kind of specimens, some local regions with lower density can be found in the wood of the lamina (Fig. 21a).

The CT analyses of specimens designated as MLCB highlight the ±45° grain orientations of the central laminae with respect to the external ones (Fig. 22). Also in this case, some defects can be found in the glue region, but it can be assumed that the presence of small amount of porosity in the glue does not affect the mechanical performance of the specimens.

6. Conclusions

Three-point bending tests have been carried out in compliance with the current EN Standards in order to assess the mechanical

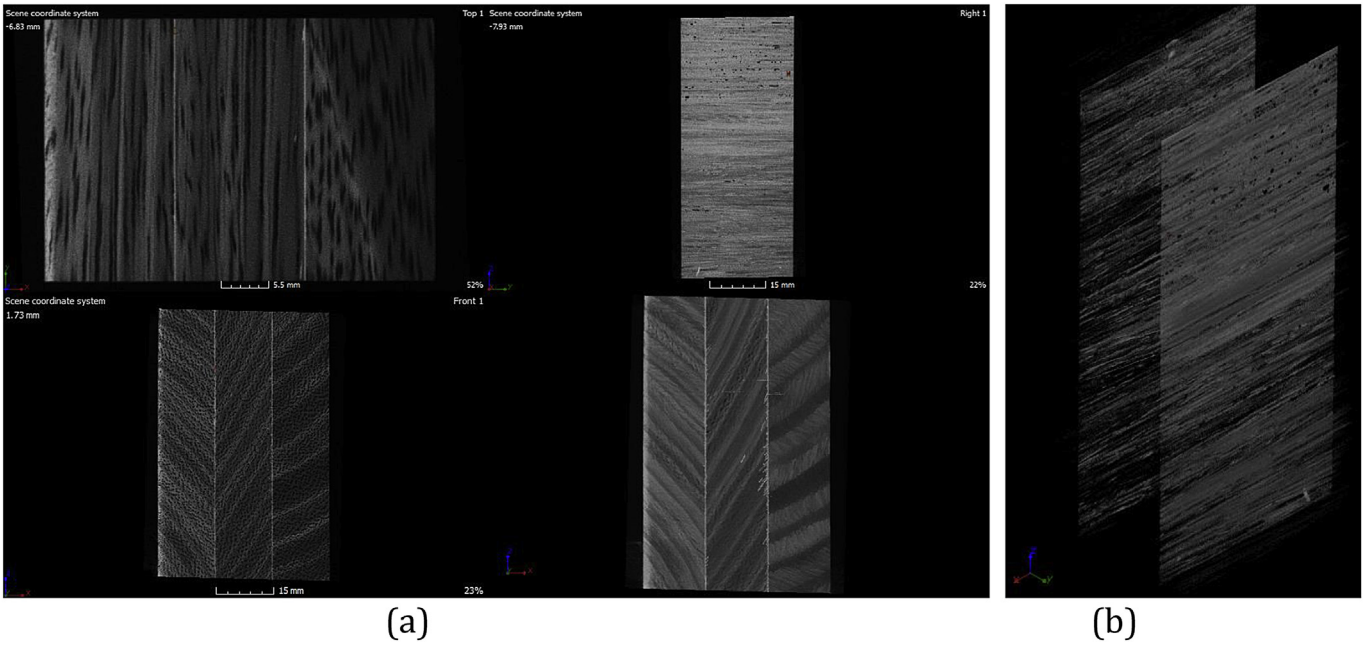

Fig. 21. Tomographic slices of the specimen without scarf joint (a); defect analysis of the glue line (b).

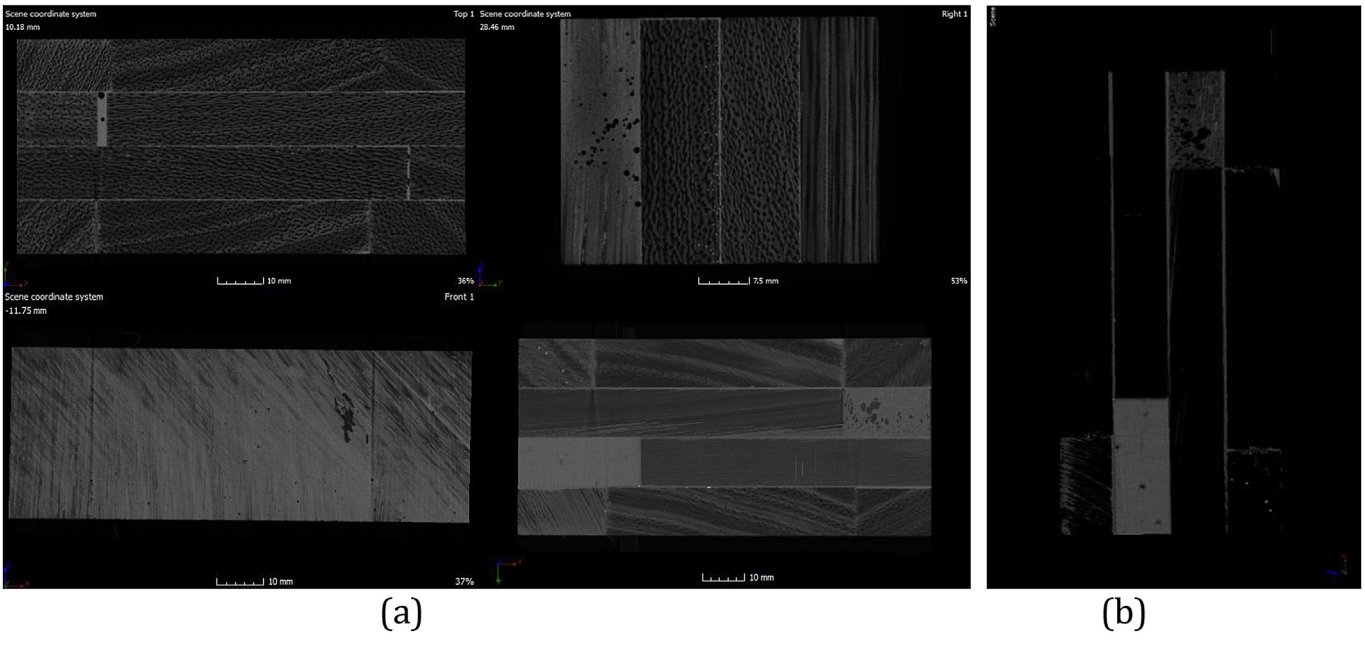

Fig. 22. Tomographic slices of the specimen consisting of 4 layers having grain orientation at 0°/±45°/0° without scarf joints. (a); defect analysis of the glue lines (b).

properties of Iroko wood laminates and the influence of scarf joints, which are the most used type of joint for wooden boats. The experimental results demonstrated that the presence of scarf joints produces a decrease of about 33% for the bending strength of the glued laminate, while the stiffness properties in terms of Young modulus in bending and shear modulus, obtained applying the "method of variable support span", remain essentially the same. The tomographic measurements of the glue thickness explained that the inhomogeneity of the glue bond-line is a reason of the reduced strength of the scarf joints. A novelty of this study is the application of the following non-destructive techniques in order to assess the presence of possible defects or voids in the adhesive region, and the dynamic modulus of elasticity: 3D computed tomography and ultrasonic phased array equipment. The value of the dynamic modulus of elasticity, evaluated by means of the ultrasonic phased array equipment, is slightly higher than the value of the modulus of elasticity obtained by the bending tests.

Moreover, theoretical approaches, based on both the Classical Lamination Theory and the Dietz method, were applied for assessing the mechanical behaviour of the laminated wood. The elastic properties and strength so estimated were validated with the experimental data, obtaining a good achievement. An interesting result of this study is that the theoretical approach based on the Dietz method, has proved to be a fast and easy way for assessing the mechanical properties of laminated wood, which are of paramount importance in the design of wooden structures.

References

[1] Taylor D. Fatigue-resistant components: what can we learn from nature? P I Mech Eng C-J Mec 2015;229:1186–93.
[2] Lucisano G, Stefanovic M, Fragassa C. Advances design solutions for high-precision woodworking machines. Int J Qual Res 2016;10(1):143–58.
[3] Fotouhi M, Saghafi H, Brugo T, Minak G, Fragassa C, Zucchelli A, et al. Effect of PVDF nanofibers on the fracture behavior of composite laminates for high-speed woodworking machines. P I Mech Eng C-J Mec 2017;231(1):31–43.
[4] Croccolo D, De Agostinis M, Fini S. Design of a cutting head for a crosscutting machine. P I Mech Eng C-J Mec 2017;231(1):5–17.
[5] Hallstrom S, Grenestedt JL. Failure analysis of laminated timber beams reinforced with glass fiber composites. Wood Sci Tech 1997;31:17–34.
[6] Mosallam AS. Structural evaluation and design procedure for wood beams repaired and retrofitted with FRP laminates and honeycomb sandwich panels. Compos Part B Eng 2016;87:196–213.
[7] Raftery GM, Kelly F. Basalt FRP rods for reinforcement and repair of timber. Compos Part B Eng 2015;70:9–19.
[8] Raftery GM, Harte AM. Nonlinear numerical modelling of FRP reinforced glued laminated timber. Compos Part B Eng 2013;52:40–50.
[9] Verma CS, Naresh Kr Sharma, Chariar VM, Maheshwari S, Hada MK. Comparative study of mechanical properties of bamboo laminae and their laminates with woods and wood based composites. Compos Part B Eng 2014;60:523e30.
[10] Shinell A, Tison T, Have HP, Structural design of s/y Dream Symphony: the largest wooden ship ever built. In: 22nd international HISWA symposium on Yacht design and Yacht construction, Amsterdam, 12–13 November 2012, pp.1–13. Edited by P.W. de Heer.
[11] Bucci V, Corigliano P, Crupi V, Epasto G, Guglielmino E, Marinò A. Experimental investigation on Iroko wood used in shipbuilding. P I Mech Eng C-J Mec 2017;231(1):128–39.
[12] Crupi V, Kara E, Epasto G, Guglielmino E, Aykul H. Prediction model for the impact response of glass fibre reinforced aluminium foam sandwiches. Int J Impact Eng 2015;77:97–107.
[13] Crupi V, Epasto G, Guglielmino E, Mozafari H, Najafian S. Computed tomography-based reconstruction and finite element modelling of honeycomb sandwiches under low-velocity impacts. J Sandw Struct Mater 2014;16:377–97.
[14] Crupi V, Epasto G, Guglielmino E. Internal damage investigation of composites subjected to low velocity impact. Exp Tech 2016;50:555–68.
[15] Crupi V, Kara E, Epasto G, Guglielmino E, Aykul H. Theoretical and experimental analysis for the impact response of glass fibre reinforced aluminium honeycomb sandwiches. first published on J Sandw Struct Mater 2016. http://dx.doi.org/10.1177/1099636216629375.
[16] Li W, Van den Bulcke J, Mannes D, Lehmann E, De Windt I, Dierick M, et al. Impact of internal structure on water-resistance of plywood studied using neutron radiography and X-ray tomography. Constr Build Mater 2014;73:171–9.
[17] Paris JL, Kamke FA. Quantitative wood–adhesive penetration with X-ray computed tomography. Int J Adhes Adhes 2015;61:71–80.
[18] Dackermann U, Elsener R, Li J, Crews K. A comparative study of using static and ultrasonic material testing methods to determine the anisotropic material properties of wood. Constr Build Mater 2016;102:963–76.
[19] Dietz AGH. Composite materials, 1965 Edgar Marburg lecture. American Society for Testing and Materials; 1965.
[20] EN 408. Timber structures – structural timber and glued laminated timber – determination of some physical and mechanical properties. CEN Euopean Committee for Standardization; 2010.
[21] EN 338. Structural timber - strength classes. CEN European Committee for Standardization; 2009.
[22] Lee CH, Chung MJ, Lin CH, Yang TH. Effects of layered structure on the physical and mechanical properties of laminated moso bamboo (Phyllosachys edulis) flooring. Constr Build Mater 2012;28(1):31–5.